International Journal of Bridge Engineering (IJBE), Vol. 1, No. 1, (2013), pp. 37-50

ANALYTICAL STUDIES OF THE SEISMIC
Performance of a Full-Scale SMA-Reinforced Bridge Column

Mostafa Tazarv[1] & M. Saiid Saiidi[2]

[1,2] Universsity of Nevada, Reno, Dept. of Civil and Environmental Engineering, USA
e-mail: mostafa.tazarv@gmail.com, saiidi@unr.edu

ABSTRACT: Residual drift under moderate and strong earthquakes has received attention because of its effect on the post-earthquake serviceability of bridges. Even though seismic codes ensure life safety for bridges, their serviceability and safety may be compromised due to large residual displacements after a severe earthquake. In this paper, a robust analytical modeling method was developed to estimate both peak and residual displacements of reinforced concrete (RC) bridge columns with high accuracy. The calculated responses showed close correlation with those measured in shake table testing of a full-scale RC bridge column. In an analytical investigation, reinforcing shape memory alloy (SMA) was used instead of conventional reinforcing steel to mitigate residual displacements. Results of cyclic and dynamic analyses of the SMA-reinforced version of the full-scale column showed that residual drifts of the SMA-reinforced concrete bridge column were significantly smaller than the calculated residual drift in the conventional RC column.

KEYWORDS: Residual displacements; RC bridge columns; Reinforcing SMA; Plastic hinge.

1 INTRODUCTION

Residual displacements have been recently emphasized as part of performance based seismic design to ensure serviceability of structures after an earthquake and reduce the rehabilitation costs. Christopoulos and Pampanin [1] proposed a direct displacement based design procedure with explicit consideration of residual displacements. Phan et al. [2] developed a framework for taking into account residual displacements in seismic design of bridge columns.

A well-designed structure may experience large residual deformations even under a design-level earthquake due to large plasticity of the reinforcements [1], making the structure unusable. For example, after the 1995 Hyogo-ken Nanbu earthquake (Japan), more than 100 reinforced concrete (RC) bridge columns experienced a tilt angle of more than 1 degree (1.75% drift). These columns had to be replaced because of the difficulty of setting the superstructure back to

the original alignments and levels [3]. It is necessary to estimate the residual displacement accurately and limit the post-earthquake drift to an acceptable value to enhance the serviceability of structures.

Analytical parameters that affect residual displacements were investigated in [4, 5, and 6]. Ruiz-Garcia and Miranda [7] and Uma et al. [8] have extended the estimation of residual deformations of structures in a probabilistic and statistical sense. Even though peak response of a structure can be estimated with a good accuracy using finite element models, an accurate calculation of residual displacement is difficult even using advanced analytical models [9]. That is, residual displacements of RC bridge columns have been successfully simulated only in a few studies [10, 11, and 12].

A few innovative methods have been proposed to mitigate residual displacements of RC bridge columns. Jeong et al. [10] replaced some of the longitudinal steel reinforcement of bridge columns with post-tensioning tendons placed at the center of the column section. The columns exhibited small residual displacements under near-fault motions in shake table tests. Iemura et al. [13] incorporated unbonded high-strength bars in RC bridge columns to increase positive post-yield stiffness, thus reducing residual displacements. Saiidi and Wang [14] explored the application of superelastic (SE) shape memory alloy (SMA) as the longitudinal reinforcements in plastic hinge of a circular RC column. Shake table testing of the SMA-reinforced column showed strong self-centering capability. Cruz and Saiidi [15] investigated the seismic performance of a large-scale four-span RC bridge incorporating innovative plastic hinges using shake table tests. The results showed minimal plastic hinge damage and small permanent deformations in the SMA-reinforced two-column bent. The literature shows that utilizing SE SMA in the plastic hinge of RC columns can effectively mitigate residual displacements.

SMA is a type of advanced material that can resist large loading cycles with negligible residual strains. The strain can be recovered upon unloading (SE effect) or by heating (shape memory effect) [16]. For application in civil engineering structures, SE behavior of SMA is of the interest. SMA remains SE at temperature above austenite finish temperature ($T \geq A_f$). Among several types of SMA alloys, Nickel-Titanium (NiTi or Nitinol) SMA has gained more interest because of its several advantages such as large strain recovery (8% strain), high energy dissipation, and excellent corrosion resistance [17].

In this paper, a robust analytical modeling method was developed to reproduce displacement history of a full-scale conventional RC bridge column tested on a shake table. Then, an analytical alternative model of the test column was developed replacing the steel reinforcement with SMA bars, while maintaining the moment capacity of the test model. A series of nonlinear analyses was performed on the SMA-reinforced concrete bridge column alternative to determine the effect of SMA reinforcement on residual displacement mitigation.

2 ANALYTICAL MODELING OF CONVENTIONAL RC COLUMN MODELS

2.1 Description of column test model

The measured response of a full-scale conventional RC bridge column (Fig. 1) tested on a uniaxial shake table at the University of California, San Diego (UCSD) [18] was used in this study for analytical model development and verification. The column clear height and diameter were 7.32 *m* (288 *in*.) and 1.22 *m* (48 *in*.), respectively. Concrete block with a weight of 2231.2 *kN* (501.6 *kips*) was used as the column head to simulate the mass. The column was reinforced longitudinally with 18-#11 (Ø36 *mm*) bars and transversely with double #5 (Ø16 *mm*) hoops spaced at 152 *mm* (6 *in*.) resulting in longitudinal and transverse steel ratios of 1.55 and 0.94%, respectively. Grade 60, A706 steel was used as the longitudinal and transverse reinforcements. The measured yield and ultimate tensile strength of the longitudinal bars were 518.5 *MPa* (75.2 *ksi*) and 706 *MPa* (102.4 *ksi*), respectively. The test day compressive strength of the column concrete was 40.9 *MPa* (5.93 *ksi*). The axial load index, which is the ratio of the axial load to the product of column gross section area and concrete compressive strength, was approximately 5%.

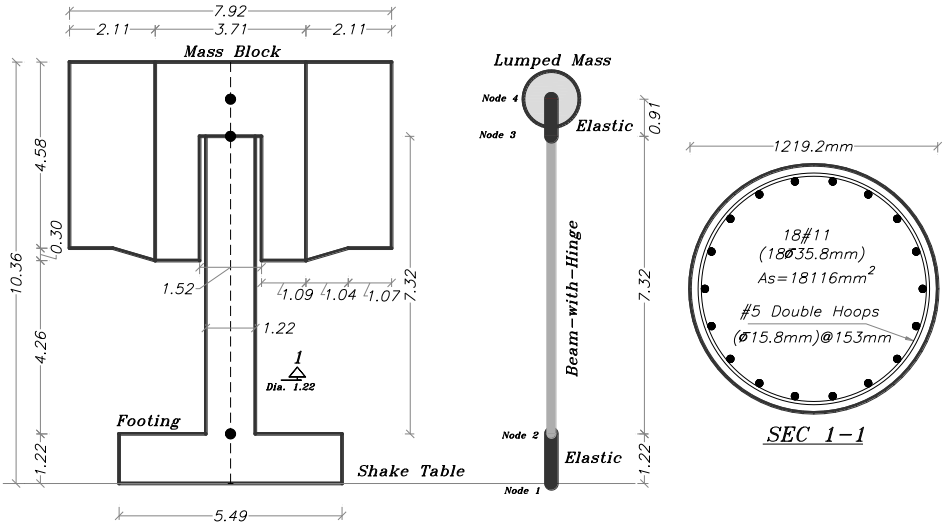

(a) (b) (c)

Figure 1. (a) Geometry of full-scale UCSD Column (unit: *m*), (b) 4-node Model, and (c) Column Section (unit: *mm*); 1 *in*.=25.4 *mm*

2.2 Description of column analytical model

A finite element computer program, OpenSees [19], was used for analyses. The footing, column, and column head were modeled utilizing a four-node three-

dimensional system (Fig. 1b). The footing and column head were modeled using elastic elements. The column was modeled utilizing a "BeamWithHinges" element, which has two plastic hinges at the element ends with a linear-elastic behavior elsewhere. The cracked stiffness ratio of the column used in the linear-elastic portion of the element was 39% of the column elastic stiffness calculated based on the Caltrans Seismic Design Criteria [20]. The length of the column base plastic hinge was 993 *mm* (39.1 *in.*) calculated using an empirical equation [21]. A fiber section was assigned to the plastic hinge. For cover concrete fibers, "Concrete02" material was used. However, "Concrete01WithSITC" material was utilized for confined core concrete. The Mander's model [22] was used to calculate the confined concrete properties. The londitidinal steel fibers were modeled with "ReinforcingSteel" material. The confined and unconfined concrete was discritized into ten-radial by ten-circumferential fibers. The mass was lumped at node 4. Forty percent of the mass of the column was also included in the lumped mass, leading to a total weight of 2311.7 *kN* (519.7 *kips*). Gravity load analysis and P-Δ analysis as the initial condition of the transient analysis were conducted first. The column was uniaxially tested under six ground motions (EQ1 to EQ6) with a range of measured peak table acceleration of 0.407 to 0.536g. The measured table accelerations were used as input motions for simulations. Rayleigh damping model was used. The damping was assumed to be proportional to the initial stiffness and the last-committed stiffness, which is the stiffness of the structure at the last committed step of analysis.

2.3 RC column simulation results

Using the above modeling approach and basic column stiffness and damping properties did not lead to good correlation between the measured and calculated displacement histories and residual displacements in any of the runs (Fig. 2). In an attempt to improve the results, the model was used to simulate each run individually. The results showed good correlation only for a few runs. For example, Fig. 3 shows the measured and calculated displacement histories of the RC column model under EQ5 using an effective stiffness ratio of 39% and a damping ratio of 3%. The model underestimated the peak and residual displacements by 14 and 7%, respectively, which are acceptable differences. The calculated displacement history also showed good correlation with the measured displacement history. However, to improve the simulation results in terms of response history correlation as well as residual displacements for each individual run, sensitivity of the calculated displacements to changes in the effective elastic stiffness of the column element and damping ratio was investigated. These parameters are important because nonlinearity is not limited to only plastic hinge of RC columns, and stiffness of columns outside the plastic hinge changes after each ground shaking. It should be noted that

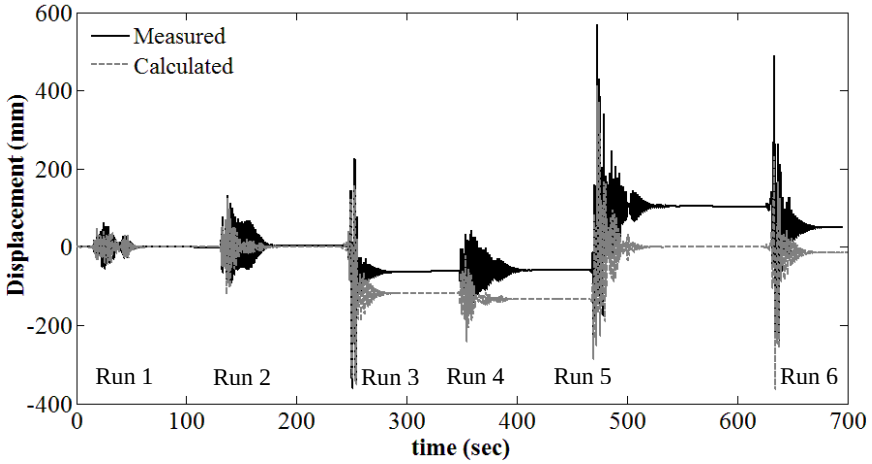

Figure 2. Measured and calculated displacement histories for all runs of RC column model with EI_{eff}=39% and damping ratio 3.0%

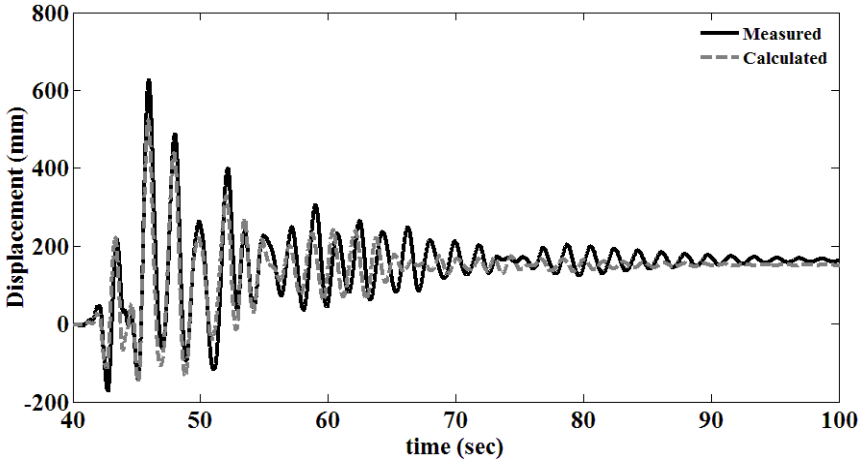

Figure 3. Measured and calculated displacement histories of RC column model only under EQ5 with EI_{eff}=39% and damping ratio 3.0%

design specifications recommend the use of cracked stiffness in analysis of RC members regardless of level of damage, number of loading cycles, and ground motion characteristics. In the sensitivity analyses, the effective stiffness had a range of 1 to 100% of the elastic stiffness of the column and the range of the damping ratio was from 1 to 5%, a common range for nonlinear analyses. Results of the sensitivity analysis for the RC column under EQ5 are shown in Fig. 4. The graphs are based on 500 dynamic analyses.

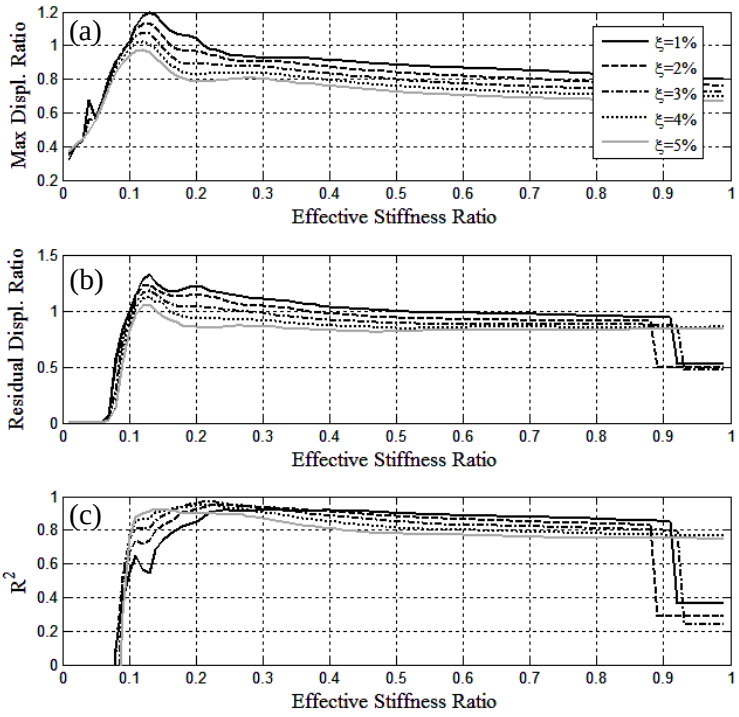

Figure 4. Variation of (a) peak displacements, (b) residual displacements, and (c) R^2 versus effective stiffness ratio for UCSD column model under EQ5

The calculated peak and residual displacements were normalized to the measured peak and residual displacements, respectively. R^2 is the coefficient of determination that shows the goodness of fit of the measured and calculated displacement histories. A R^2 value of one indicates perfect fit. In the figure, the normalized responses were plotted versus the effective stiffness using different damping ratios. It can be seen that the best displacement history match (R^2 ≈1.0) can be achieved if the effective stiffness ratio is approximately 20% (Fig. 4c). Then, the critical step is to choose a damping ratio. In this run, a single damping ratio could not lead to satisfactory correlation in both maximum and residual displacement. Since the interest of this paper was residual displacement, a damping ratio of 3.2% was used because it led to the best residual displacement match (Fig. 4b). A simulation for this run using an effective stiffness ratio of 19% and a damping ratio of 3.2% led to 12% underestimation of the peak displacement, 1% overestimation of the residual displacement, and near perfect match for the displacement history (R^2=0.95).

It is clear that by modifying the effective linear stiffness and damping ratio for each run, the best correlation between the calculated and measured displacement histories can be achieved. Therefore, a similar procedure was

used to optimize simulation results for the other runs. Figure 5 shows the measured and calculated displacement histories for all runs. Table 1 presents the optimized modeling parameters and the calculated and measured peak and residual displacements for all the runs. Note that the measured and calculated residual displacements were the mean displacements of the last 10 seconds during free vibration. Overall, it can be seen that using appropriate damping ratio and effective stiffness, it is possible to simulate the measured displacement history of all runs with high accuracy.

In addition to the displacement history, the model was able to reproduce the other measured responses with sufficient accuracy. For example, measured and calculated base shear histories of the column under EQ5 is shown in Fig. 6, which shows a good correlation. Since the RC column experienced the highest peak and residual displacements under EQ5, only the analytical model and parameters (Table 1) pertaining to this run was used for further analyses.

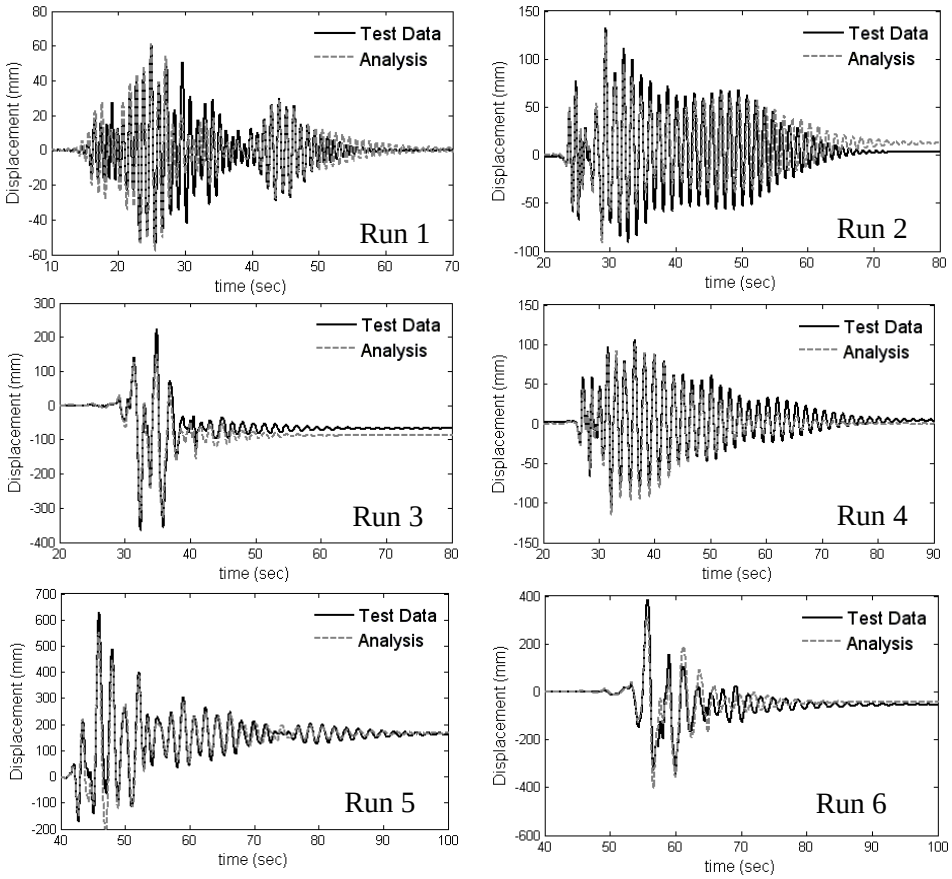

Figure 5. Measured and calculated displacement histories for UCSD column

Table 1. Measured and calculated displacements of UCSD column

Earthquake	EI_{eff}/EI_g*	Damping Ratio, ξ (%)	Measured Peak Disp. *(mm)*	Calculated Peak Disp. *(mm)*	Measured Residual Disp.$^+$ *(mm)*	Calculated Residual Disp.$^+$ *(mm)*	R^2
EQ1	0.75	2.0	60.9	61.3	0.0	0.0	0.60
EQ2	0.48	2.5	132.2	127.1	3.2	12.9	0.61
EQ3	0.30	5.0	-46.6	-30.8	-67.4	-87.8	0.85
EQ4	0.18	3.0	-106.9	-114	4.2	0.0	0.91
EQ5	0.19	3.2	628.2	551.8	163.6	165.8	0.95
EQ6	0.13	5.0	385.1	-404.9	-54.4	-43.4	0.77

* Only for linear-elastic portion of "BeamWithHinges" element (column element)
$^+$ Mean of the last 10-second of free vibration

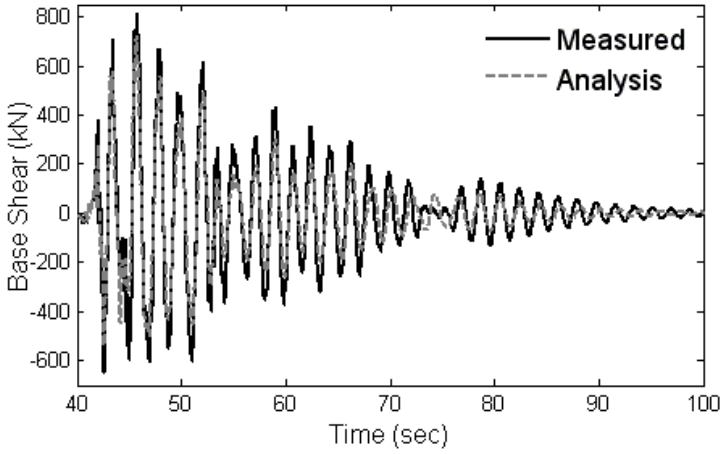

Figure 6. Measured and calculated base shear histories for UCSD column under EQ5

3 ANALYTICAL MODELING OF SMA-REINFORCED COLUMN MODELS

3.1 Reinforcing SMA model

Tazarv and Saiidi [23] proposed a design specification for NiTi SE reinforcing SMA bars. Figure 7 shows the NiTi SE SMA model parameters and Table 2 presents the expected mechanical properties. This symmetric SMA model was used in this study. "SelfCentering" material was used in OpenSees for SMA fibers.

3.2 SMA-reinforced column simulation results

A series of moment-curvature analyses showed that the flexural strength of a column with similar geometry, detailing, and material strength compared to the conventional column test model but longitudinally reinforced with 24-#11 (Ø36 *mm*) SMA bars is the same as that of the conventional column test model.

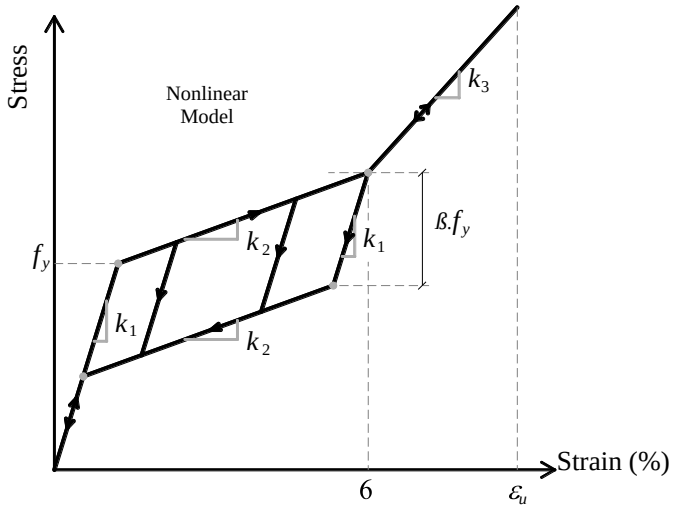

Figure 7. Nonlinear model for NiTi SE SMA [23]

Table 2. Expected reinforcing NiTi SE SMA mechanical properties

Parameter	Expected
Austenite modulus, k_1	5500 *ksi* (37900 *MPa*)
Post yield stiffness, k_2	250 *ksi* (1725 *MPa*)
Austenite yield strength, f_y	55 *ksi* (380 *MPa*)
Lower plateau stress factor, β	0.65
Recoverable superelastic strain, ε_r	6%
Secondary post-yield stiffness ratio, $\alpha=k_3/k_1$	0.3
Ultimate strain, ε_u	10%

Figure 8 shows the calculated force-drift hysteretic relationship of the conventional and SMA-reinforced columns. The SMA bars were only used in the plastic hinge of the column. The drift is the ratio of the column lateral displacement to the column height. It can be seen that the strength of both columns are the same. However, the SMA-reinforced column exhibits very small residual displacements even under large displacement cycles. Here "residual displacement" refers to the displacement at the intersection of the unloading curves with the abscissa. Figure 9 shows the residual drift ratio versus the peak drift ratio for both columns. The SMA-reinforced column exhibited 80% lower residual displacements at each drift level on average compared to the conventional column. Figure 10 shows displacement history of the conventional and SMA-reinforced column models under EQ5. In the SMA-reinforced column, the peak displacement demand was increased by 22% while the residual displacement was reduced by 63% compared to the conventional column.

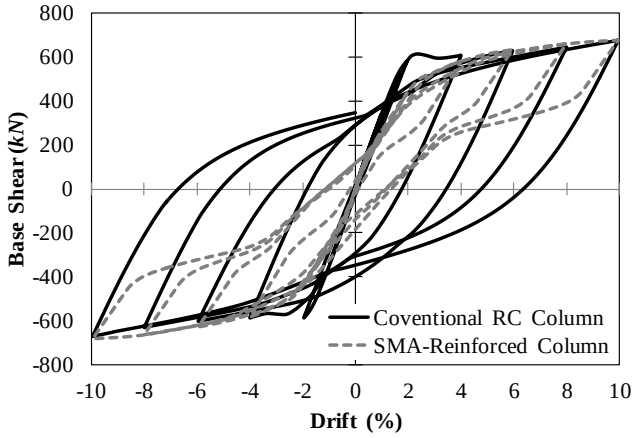

Figure 8. Force-drift hysteretic relationship of conventional and SMA-reinforced columns

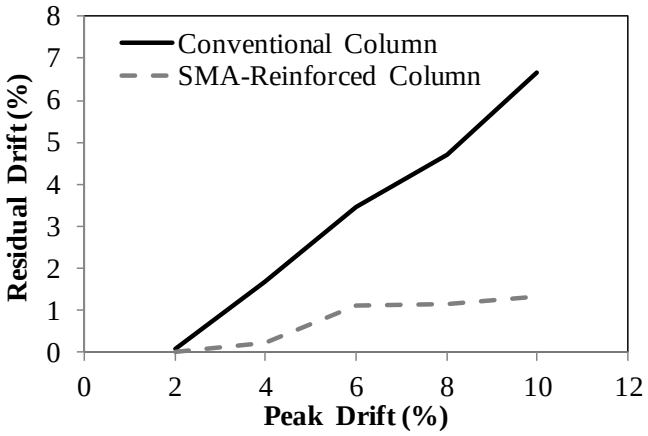

Figure 9. Residual drift versus peak drift of conventional and SMA-reinforced columns

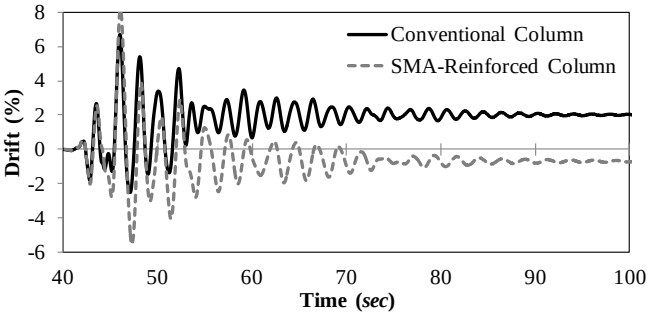

Figure 10. Displacement history of conventional and SMA-reinforced columns under EQ5

3.3 SMA-reinforced column under near-fault motions

Structures are known to be particularly susceptible to the impulsive nature of the fault-normal component of near-fault earthquakes. To investigate the effect of SMA bars on the reduction of residual displacements under near-fault earthquake motions, a series of response history analyses was performed using 10 near-fault ground motion records [24]. Table 3 presents the characteristics of the motions. The fault-normal component of each record was used in analyses because this component has a large pulse-like velocity, typically causing significant residual displacement. The effective stiffness ratio and damping ratio for both conventional and SMA-reinforced column models were 19% and 3.2%, respectively.

Table 3. Near-field records [24]

EQ. No.	Earthquake	PGA (g)	PGV (cm/s)	Station	Location & Date	M_s	Distance (*km*)
1	Tabas	0.88	114.5	Tabas	IRAN, 16/09/78	7.4	1.2
2	Loma Prieta	0.74	134.8	Los Gatos	US., 17/10/89	7.0	3.5
3	Loma Prieta	0.76	151.3	Lexington Dam	US., 17/10/89	7.0	6.3
4	C. Mendocino	0.73	141.4	Petrolia	US., 07/06/92	7.1	8.5
5	Erzincan	0.448	85.3	Erzincan	Turkey, 03/13/92	6.7	2
6	Landers	0.714	94.5	Lucerne	US, 06/28/92	7.3	1.1
7	Nothridge	0.94	139.3	Rinaldi	US, 01/17/94	6.4	7.5
8	Nothridge	0.72	101.8	Olive View	US, 01/17/94	6.4	7.5
9	Kobe	1.02	167.8	JMA	Japan, 01/16/95	6.9	3.4
10	Kobe	0.73	168.5	Takatori	Japan, 01/16/95	6.9	4.3

Figure 11 shows the peak and residual drifts for the conventional and SMA-reinforced columns under the near-fault motions. It can be seen that the trend in the peak displacements for two column models was similar but the peak displacement of the SMA-reinforced column was 13% higher than the conventional column on average. The residual displacements, however, were substantially lower when SMA bars were used. The SMA bars reduced residual displacements by an average of 97% compared to the conventional column. The Japanese seismic design specifications for highway bridges limit the residual drift ratio to 1% [3]. The analytical results show that the conventional RC bridge column fails to meet this limitation under 7 out of the 10 earthquakes. However, the SMA-reinforced column meets the limitation for all the ground motions. It is clear that SMA longitudinal bars are very effective in minimizing residual drifts and improving post-earthquake serviceability of bridges.

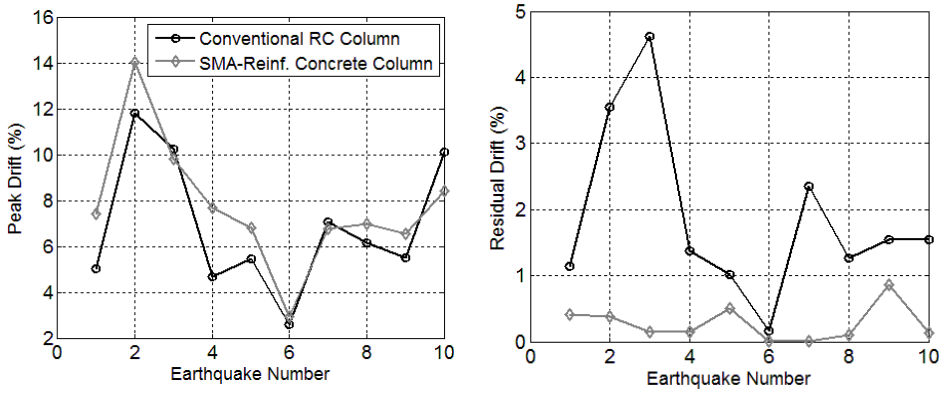

(a) peak drift (b) residual drift

Figure 11. Peak and residual drifts for conventional and SMA-reinforced columns under near-field motions

4 CONCLUSIONS

A robust analytical modeling method was developed to reproduce the response histories of a full-scale reinforced concrete bridge column under earthquake loading with emphasis on residual displacements. The basic model was not generally able to reproduce the response histories for different runs with acceptable accuracy. To improve the simulation of displacement histories and residual displacements, the effective stiffness ratio of the linear-elastic portion of the column element as well as the Rayleigh damping ratio were modified for each individual run leading to good correlation of the calculated and measured responses for all six runs. The verified analytical model was used to investigate the effect of SMA longitudinal bars on the seismic performance of the column. The results of various nonlinear analyses showed that the SMA bars incorporated only in the plastic hinge of the bridge column can substantially reduce residual drifts, thus ensuring the post-earthquake functionality of the bridge.

ACKNOWLEDGMENTS

The study presented in this paper was funded by the California Department of Transportation (Caltrans) through contract No. 65A0372. Special thanks are due Dr. Saad El-Azazy and Dr. Charles Sikorsky, the Caltrans Research Program Managers for their support and advice.

REFERENCES

[1] Christopoulos, C, and Pampanin, S, "Towards Performance-based Seismic Design of MDOF Structures with Explicit Consideration of Residual Deformations", *ISET Journal of Earthquake Technology*, Paper No. 440, Vol. 41, No. 1, pp. 53-73, 2004.

[2] Phan, V, Saiidi, MS, Anderson, J, and Ghasemi, H, "Near-Fault Ground Motion Effect on Reinforced Concrete Bridge Columns", *Journal of Structural* Engineering, ASCE , Vol. 33, No. 7, pp. 982-989, 2007.
[3] Kawashima, K, "Seismic Design and Retrofit of Bridges", *Proc. of 12th World Conference on Earthquake Engineering*, New Zealand Society for Earthquake Engineering, CD-ROM No. 2828. Auckland, New Zealand, 2000.
[4] MacRae, GA, Kawashima, K, "Post-Earthquake Residual Displacements of Bilinear Oscillators", *Earthquake Engineering and Structural Dynamics*, Vol. 26, pp. 701–716, 1997.
[5] Borzi, B, Calvi, GM, Elnashai, AS, Faccioli, E, Bommer, J, "Inelastic Spectra for Displacement-Based Seismic Design", *Soil Dynamics and Earthquake Engineering*, Vol. 21, No.1, pp.47–61, 2001.
[6] Christopoulos, C, Pampanin, S, Priestley, MJN, "Performance-Based Seismic Response of Frame Structures Including Residual Deformations. Part I: Single-Degree-of-Freedom Systems', *Journal of Earthquake Engineering*, Vol. 7, No. 1, pp. 97–118, 2003.
[7] Ruiz-Garcia, J, Miranda, E, "Residual Displacement Ratios for Assessment of Existing Structures", *Earthquake Engineering and Structural Dynamics*, Vol. 35, No. 3, pp. 315–336, 2006.
[8] Uma, SR, Pampanin, S, Christopoulos, C, "A Probabilistic Framework for Performance-Based Seismic Assessment of Structures Considering Residual Deformations", *Proceedings of the 1st ECEES*, Paper 731. Geneva, Switzerland, 2006.
[9] Yazgan, U, and Dazio, A, "Simulating Maximum and Residual Displacements of RC Structures: I. Accuracy", *Earthquake Spectra*, EERI, Vol. 27, No. 4, pp. 1187-1202, 2011.
[10] Jeong, HIL, Sakai, J, Mahin, SA, "Shaking Table Tests and Numerical Investigation of Self-Centering Reinforced Concrete Bridge Columns", *PEER-2008/06*, Pacific Earthq. Engrg. Res. Center, Univ. of California at Berkeley, California, 2008.
[11] Kwan, WP, Billington, SL, "Unbonded Post-Tensioned Concrete Bridge Piers. I: Monotonic and Cyclic Analyses", *Journal of Bridge Engineering*, ASCE, Vol. 8, No. 2, pp. 92-101, 2003a.
[12] Saiidi, M, and Seyed Ardakani, SM, "An Analytical Study of Residual Displacements in RC Bridge Columns Subjected to Near-Fault Earthquakes", *Bridge Structures*, Vol. 8, pp. 35-45, 2012.
[13] Iemura, H, Takahashi, Y, Sogabe, N, "Development of Unbonded Bar Reinforced Concrete Structure", *Proceedings of 13th World Conference on Earthquake Engineering*, Paper 1537. Vancouver, B.C., Canada, 2004.
[14] Saiidi, MS, and Wang H, "Exploratory Study of Seismic Response of Concrete Columns with Shape Memory Alloys Reinforcement", *ACI Structural Journal*, Vol. 103, No. 3, pp. 436-443, 2006.
[15] Cruz Noguez, CA, and Saiidi, MS, "Shake Table Studies of a 4-Span Bridge Model with Advanced Materials", *Journal of Structural Engineering*, ASCE , Vol. 138, No. 2, pp. 183-192, 2012.
[16] Otsuka, K, and Wayman, CM, "Mechanism of Shape Memory Effect and Superplasticity", Cambridge University Press, Cambridge, U.K., pp. 27–48, 1998.
[17] Alam, M.S., Nehdi, M. and Youssef, M.A. (2009). Seismic Performance Of Concrete Frame Structures Reinforced With Superelastic Shape Memory Alloys. Smart Structures and Systems , Vol. 5, No. 5, 565-585.
[18] Concrete Column Blind Prediction Contest, http://nisee2.berkeley.edu/peer/prediction_contest, 2010.
[19] OpenSees, "Open System for Earthquake Engineering Simulations", Version 2.4.1, Berkeley, CA, Available online: http://opensees.berkeley.edu, 2013.
[20] Caltrans, "Seismic Design Criteria (SDC)", version 1.4, Sacramento, CA, California Department of Transportation, 2006.
[21] Paulay, T, and Priestley, MJN, "Seismic Design of Reinforced Concrete and Masonry

Buildings", New York: Wiley, 1992.
[22] Mander, JB, Priestley, MJN, Park, R, "Theoretical Stress-Strain Model for Confined Concrete", *Journal of Structural Engineering*, ASCE , Vol. 114, No. 8, pp. 1804-1826, 1988.
[23] Tazarv, M, and Saiidi, MS, "Reinforcing NiTi Superelastic SMA for Concrete Structures", Submitted to *Journal of Structural Engineering*, ASCE , Vol. xx, No. xx, pp. xx-xx.
[24] Somerville, P, Smith, N, Punyamurthula, S, Sun, J, "Development of Ground Motion Time Histories for Phase 2 of the FEMA/SAC Steel Project", *Report No. SAC/BD-97/04*, SAC Joint Venture, California, 1997.

Received: Dec. 22, 2013 Accepted: Dec. 27, 2013